ACS Partner Journal

CHEM & BIO ENGINEERING

pubs.acs.org/ChemBioEng

Article

Two-Step Synthesis of a Dolutegravir Intermediate DTG-6 in a Microfluidized Bed Cascade System: Route Design and Kinetic Study

Xiao Xue, Chengmin Xie, Guozhi Qian, Minjing Shang,* Min Qiu, Rongkun Jiang, Mohsin Pasha, Zihao Zhong, Zhijun Wang, Shu Liu, Hua Zhang, and Yuanhai Su*

Cite This: *Chem Bio Eng.* 2025, 2, 182−191

Read Online

ACCESS | Metrics & More | Article Recommendations | Supporting Information

ABSTRACT: In the existing two-step method for the preparation of DTG-6 (i.e., an important intermediate of the anti-HIV drug Dolutegravir (DTG)), a strong base is required to neutralize the homogeneous strong acid catalyst of the first step to make the reaction solution weakly acidic for the DTG-5 cyclization in the second step. The DTG-6 yield in the two-step synthesis is affected by the reaction of the strong base with the carboxyl group on the generated intermediate DTG-5. In this article, a solid acid catalyst, titanium cation-exchanged montmorillonite (Ti^{4+}-mont), was used in the microfluidized bed to catalyze the conversion of DTG-4 to DTG-5. DTG-5 can be directly cyclized with (*R*)-3-aminobutanol (RABO) to form DTG-6 without the introduction of a strong base into the reaction solution. After the parametric screening on the flow rate, solid acid type, temperature, residence time, and solvent type, the DTG-6 yield increased from 90% (in our previous work) to 95% in the microfluidized bed cascade system. Due to the easy separation of heterogeneous catalyst, the utilization of a microfluidized bed not only simplified operations, but also improved synthetic efficiency. Moreover, the kinetics of the cyclization of unstable intermediate DTG-5 with RABO was investigated and verified by means of experimental data.

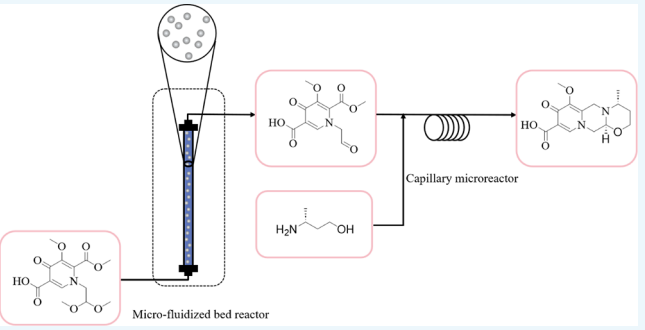

KEYWORDS: *Dolutegravir, microfluidized bed, kinetics, deprotection of acetal, cyclization*

1. INTRODUCTION

To date, about 39 million people are living with human immunodeficiency virus (HIV) around the world, which is a major challenge for global public health.[1] Integrase strand transfer inhibitor (INSTI) can block the integration of viral deoxyribonucleic (DNA) into host cell DNA, which is the necessary step in the replication cycle of HIV.[2] The benefits of the second-generation INSTI Dolutegravir (DTG, brand name Tivicay[3]) over the first-generation INSTIs (e.g., raltegravir[4] and elvitegravir[5]) include lower doses,[6] less adverse effects,[7] and higher resistance.[8] The synthesis route (Figure 1) of DTG, beginning with methyl 4-methoxy-3-oxobutanoate, was published by GlaxoSmithKline.[9]

In this route, methyl 4-methoxy-3-oxobutanoate was converted to vinylogous amide by the condensation and substitution reaction, followed by the cyclization and selective hydrolysis reaction to obtain intermediate DTG-4. Acetal DTG-4 then was deprotected to intermediate DTG-5 under catalysis with methanesulfonic acid. Acetals are widely used to protect carbonyl groups in synthetic organic chemistry, and thus there are many studies on forming and deprotecting them.[10] Many catalysts can be applied in the deprotection of acetals, such as Lewis acids,[11] molecular iodine,[12] bismuth nitrate pentahydrate,[13] etc. In the process of DTG-4 deprotection, excellent DTG-5 yield was easily obtained through catalysis by strong acids (e.g., p-TsOH·H_2O[14] and methanesulfonic acid[15]). In particular, 100% DTG-5 yield could be achieved within 0.5 min in the microreactor using formic acid as a catalyst.[16] Subsequently, the reaction solution containing DTG-5 was directly reacted with (*R*)-3-aminobutanol (RABO, the reactant in the DTG-5 cyclization) to afford DTG-6 in the microreactor system. The best results of the two-step method afforded 71% DTG-6 yield when using acetic/methanesulfonic acid and 34% DTG-6 yield when using formic acid.[16] Due to the side reaction between the strong acid (the catalyst in the DTG-4 deprotection) and RABO, the two-step process produced a high content of complex byproducts and affected the yield of DTG-6. In our previous study,[17] the reaction solution containing DTG-5 was first mixed with a base, through which the catalyst strong acid underwent neutralization reaction to create a weakly acidic environment.

Received: August 24, 2024
Revised: October 27, 2024
Accepted: October 29, 2024
Published: November 12, 2024

https://doi.org/10.1021/cbe.4c00139
Chem Bio Eng. 2025, 2, 182−191

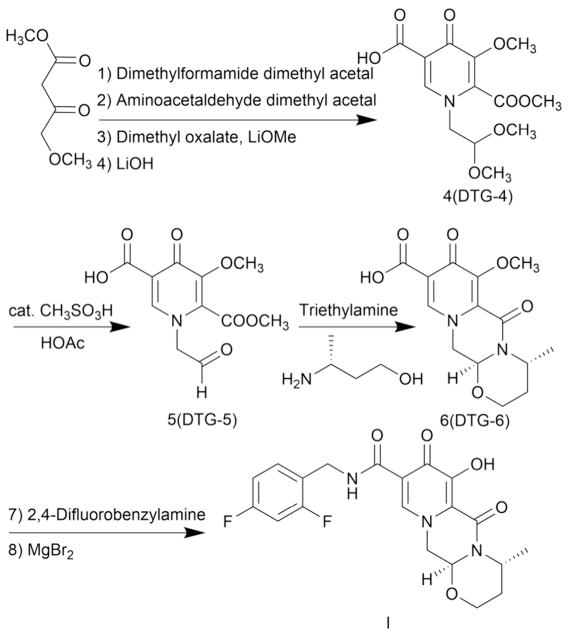

Figure 1. Schematic representation of the DTG synthesis route.

The weakly acidic reaction solution then was mixed with another reaction solution containing RABO to prepare DTG-6 by cyclization. The total yield of DTG-6 synthesized by the two-step process in a cascade capillary microreactor system could reach 90% with a residence time of 50 min,[17] and the results indicated that a weakly acidic environment is required for the DTG-5 cyclization. Therefore, it is necessary to introduce the base to adjust the reaction solution containing DTG-5 to a weak acidity when a strong acid is employed as the catalyst in the DTG-4 deprotection. When a strong base was introduced to neutralize the strong acid, it would react with the generated intermediate DTG-5 containing carboxyl group to decrease the concentration of DTG-5 and the DTG-6 yield.[17] This is the main reason that the current DTG-6 yield does not exceed 90%. Meanwhile, this method has drawbacks including difficult separation of catalyst and product, and cumbersome post-treatment.[18]

To further improve the DTG-6 yield, it is essential to avoid the introduction of a strong base in the two-step reaction process. Therefore, we propose solving this problem with a heterogeneous catalyst. Compared with the disadvantages of homogeneous catalysts (the difficulty of product separation and the generation of unrecoverable salt waste), heterogeneous catalysts allow for continuous utilization, eliminating tedious separation and reducing production cost. At the same time, the heterogeneous catalysts have their own advantages over the homogeneous catalysts, such as lower cost and easier storage.[19] Due to financial advantages and environmental protection, the application of heterogeneous catalytic systems in synthesis has received increasing attention from academia and industry in recent years.[20] Over the past decades, microreactor applications have expanded rapidly in a variety of fields such as functional materials, energy, and fine chemicals,[21] owing to its advantages such as fast heat and mass transfer,[22] enhanced process safety,[23] and precise control over operational parameters. Therefore, we combined the microreactors with heterogeneous catalysts to study DTG-4 deprotection. Although Nqeketo and Watts[16] attempted to utilize acidic resin catalysts to catalyze the DTG-4 deprotection in a micro packed-bed reactor, the method was abandoned for the low DTG-5 selectivity (48%). Considering the particle size of the catalysts (micrometer scale), the consumption of catalysts, the pressure drop over the reactor, and the stable operation of the system, we searched for a suitable solid acid catalyst to build a microfluidized bed to solve the problem instead of a micro packed-bed reactor. In 1982, Scott et al.[24] first studied the biomass pyrolysis in a small fluidized reactor with an internal diameter of 8 mm. However, the concept of microfluidized beds in liquid−solid systems was first introduced by Potic et al.[25] In 2005. Microfluidized beds are made of various metals or quartz and can be operated at high temperatures. Especially for quartz reactors, it is convenient for experimenters to observe the operating state inside the microfluidized beds at any time. Microfluidized beds have the advantages of well-controlled hydrodynamics and low amount of catalysts required.[26−28] Also, mixing and mass transfer in microfluidized beds are enhanced resulting from the presence of particles.[29] Microfluidized bed cascade systems with heterogeneous catalysts are suitable for multistep organic synthesis processes requiring various pH values of reaction solutions,[30−32] which can avoid introducing unwanted compounds to adjust the pH. In addition, microfluidized bed reactors have been used in catalytic cracking, photocatalysis, oxidation, and so on.

For the first time, this work presents a highly selective two-step synthesis of DTG-6 utilizing a heterogeneous catalyst in a microfluidized bed cascade system. Meanwhile, the effects of different parameters (e.g., solid acid, solvent, and temperature) on the DTG-4 deprotection and DTG-5 cyclization were independently investigated in the microfluidized bed system. In this work, DTG-6 yield was improved from 90% (highest yield in the literature) in the cascade capillary microreactor system[17] to 95% in the microfluidized bed cascade system, which confirmed the efficient intensification of the pharmaceutical synthesis. The kinetic parameters of the DTG-5 cyclization were further established and validated based on the experimental data. The solid acid catalyst Ti^{4+}-mont running for 18 h could be reused after post-treatment. It is sustainable to search for an appropriate solid acid catalyst and optimize process operations to obtain a high DTG-6 yield and selectivity. Such a microfluidized bed cascade system is also suitable to other multistep reactions with strict acidity requirements.

2. EXPERIMENTAL SECTION

2.1. Materials. $TiCl_4$ (99.5%), ammonia solution (28 wt %), ethyl silicate (42 wt %), ethanol (99.7%), methanes ulfonic acid (99%), and Na-montmorillonite ($Na_{0.66}(OH)_4Si_8(Al_{3.34}Mg_{0.66}Fe_{0.19})O_{20}$, Na-mont, RG) were all obtained from Shanghai Aladdin Bio-Chem Technology Co., Ltd. *N*,*N*-Dimethylformamide (DMF, 99.5%), acetic acid (AcOH, 36 wt %), acetonitrile (ACN, 99.5%), dimethyl sulfoxide (DMSO, 99.8%), acetone (99.5%), and sulfuric acid (98%) were procured from Shanghai Titan Scientific Co., Ltd., China. RABO (99.9%), DTG-4 (99.9%), and DTG-6 (99.9%) were purchased from Shanghai Desano Pharmaceuticals Co., Ltd., China. The chemicals purchased were used as received without further purification.

2.2. Preparation of Solid Acid Catalysts. Titanium cation-exchanged montmorillonite (Ti^{4+}-mont) was a strong solid acid prepared from $TiCl_4$ and montmorillonite, which efficiently catalyzed the etherification of alcohols,[33] the esterification of carboxylic acids,[34] the acetalization of carbonyl compounds,[35] and the aromatic alkylation.[36] The 1.8 mol/L $TiCl_4$ solution was prepared by slowly adding $TiCl_4$ dropwise to a flask containing water, which was immersed in an ice water bath. 3 g of Na-mont was added to the prepared $TiCl_4$ solution at 50 °C. Following stirring for 24 h, the

https://doi.org/10.1021/cbe.4c00139
Chem Bio Eng. 2025, 2, 182−191

suspension was filtered and washed to remove chloride ion with 1000 mL of deionized water. The off-white solid, i.e., Ti^{4+}-mont solid acid, was obtained after drying for 8 h at 110 °C. In addition, some other solid acid catalysts were produced.

The pH of the $TiCl_4$ solution was adjusted to 9−10 by slowly adding 6 mol/L dilute ammonia solution. After aging for 24 h, the precipitate was washed with deionized water to ensure the absence of a chloride ion. It was dried at 50 °C and then ground into a powder. The powder was added to 0.5 mol/L sulfuric acid solution under ultrasonic stirring and soaked for 30 min, after which it was filtered and dried at 80 °C. Afterward, it was calcined and activated at 500 °C for 3 h to obtain the SO_4^{2-}/TiO_2 solid super acid.[37]

Another solid acid catalyst prepared was silica-supported methanesulfonic acid. 65 mL of ethyl silicate and 6 mL of methanesulfonic acid were slowly added into the mixed solution of 100 mL of ethanol and 100 mL of distilled water, which was stirred at 80 °C until a gel appeared. The gel was cooled and then dried at 90 °C for 24 h. It was ground and sieved to form particles with the size of 180−250 μm. The solid particles then were calcined at 200 °C for 24 h to acquire silica-supported methanesulfonic acid.[38]

2.3. Experimental Setup and Procedure. *2.3.1. Synthesis of DTG-5 via DTG-4 Deprotection Catalyzed by Solid Acid Catalyst in the Microfluidized Bed.* The experimental setup of the microreactor system containing solid acid as the fluidized particles for the deprotection of DTG-4 is shown in Figure S1. A 0.2 g portion of solid acid catalyst was added to the steel column with 4.6 mm inner diameter, and two mesh screens at each end of the column could stop the catalyst from flowing away. In addition, the inner diameter of the perfluoroalkoxy (PFA) capillaries connected to the steel column was 1.0 mm. The 0.1 mol/L DTG-4 solution was introduced into the vertically placed steel column by a syringe pump (Ne-1600, New Era Pump Systems Inc., U.S.). The reaction temperature was set between 105 and 120 °C. The residence time t_1 was controlled by changing the length of the steel column and the volumetric flow rate of the reaction solution. A back pressure regulator (1 mm ID, IDEX Health & Science Co. Ltd.) kept the pressure in the microreactor system constant at levels up to 2.76 bar. After the process reached a stable state, the sample from the outlet of the microreactor system was collected into a volumetric flask containing ACN. High performance liquid chromatography (HPLC, Shimadzu LC-16, Japan) was applied to analyze the samples. Each experiment was repeated three times to control the experimental errors within ±2%, and the average value was adopted as the final data.

2.3.2. Synthesis of DTG-6 by DTG-5 Cyclization in the Microreactor. Solution A, i.e., an acetic acid solution with the DTG-5 concentration of 0.2 mol/L, and solution B, i.e., the ACN solution with 1.08 equiv of RABO, were mixed via a polyether ether ketone (PEEK) T-mixer (Figure S2). Solutions were introduced into the capillary microreactor by springe pumps to undergo the cyclization at pressure of 2.76 bar, and the capillary microreactor was placed into an oil bath to control the reaction temperature at 95−135 °C. The flow rates of solution A and solution B were both 0.03 mL/min. t_2 represents the residence time of cyclization in the capillary microreactor.

2.3.3. Two-Step Synthesis of DTG-6 from DTG-4 in the Microfluidized Bed Cascade System. Two reaction processes mentioned above were combined to build the microfluidized bed cascade system to prepare DTG-6, and the corresponding schematic diagram of the experimental setup is shown in Figure 2. The acetic acid solution (solution C) containing 0.1 mol/L DTG-4 was introduced into microreactor 1 (the microfluidized bed with 0.4 g of solid acid catalyst) by a piston pump (Xingda 2PB-00D, China) at a flow rate of 0.03 mL/min to synthesize DTG-5. The reaction temperature was 120 °C, and the bed voidage was 0.6. Upon further mixing of the reaction solution containing DTG-5 with solution D (ACN solution containing RABO) via a T-mixer, DTG-6 was generated at 135 °C by cyclization in PFA capillary microreactor 2. The flow rate of solution D was also 0.03 mL/min. The total residence time for the two-step method was expressed as t_3. Both microreactor 1 and microreactor 2 were immersed in an oil bath to control the reaction temperature and were equipped with a 2.76 bar back pressure regulator behind them.

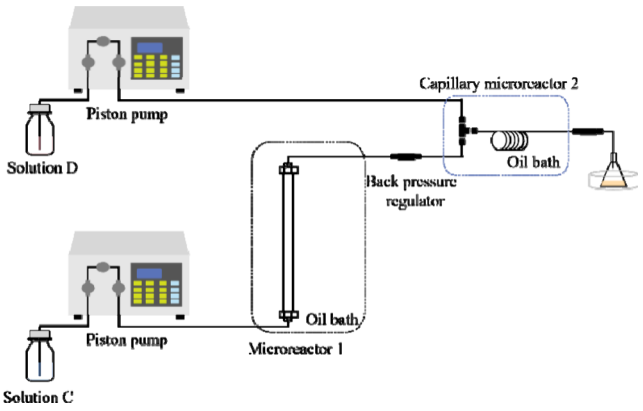

Figure 2. Schematic diagram for the two-step synthesis of DTG-6 from DTG-4 in the microfluidized bed cascade system.

2.4. Analysis. The concentrations of DTG-4, DTG-5, and DTG-6 were measured by HPLC.[17] The column temperature was set at 308 K, and the injection volume was 2 μL. The eluent was a mixture of ACN and deionized water, and the volume percentage of ACN was increased from 5% to 95% in 25 min with a linear gradient elution. The eluent flow rate was set at 1 mL/min, and the wavelength of the UV detector was set to 282 nm.

2.5. Definitions. The conversion of DTG-4 and DTG-5, the yield of DTG-5 and DTG-6, and the corresponding selectivity in independent reactions were defined by

$$\text{DTG-4 conversion: } X_{\text{DTG-4}} = \frac{C_{\text{DTG-4-0}} - C_{\text{DTG-4}}}{C_{\text{DTG-4-0}}} \quad (1)$$

$$\text{DTG-5 conversion: } X_{\text{DTG-5}} = \frac{C_{\text{DTG-5-0}} - C_{\text{DTG-5}}}{C_{\text{DTG-5-0}}} \quad (2)$$

$$\text{DTG-5 yield: } Y_{\text{DTG-5}} = \frac{C_{\text{DTG-5}}}{C_{\text{DTG-4-0}}} \quad (3)$$

$$\text{DTG-6 yield: } Y_{\text{DTG-6}} = \frac{C_{\text{DTG-6}}}{C_{\text{DTG-5-0}}} \quad (4)$$

$$\text{DTG-5 selectivity: } S_{\text{DTG-5}} = \frac{Y_{\text{DTG-5}}}{X_{\text{DTG-4}}} \quad (5)$$

$$\text{DTG-6 selectivity: } S_{\text{DTG-6}} = \frac{Y_{\text{DTG-6}}}{X_{\text{DTG-5}}} \quad (6)$$

where $C_{\text{DTG-4}}$, $C_{\text{DTG-5}}$, and $C_{\text{DTG-6}}$ represent the concentrations of DTG-4, DTG-5, and DTG-6, respectively. $C_{\text{DTG-4-0}}$ and $C_{\text{DTG-5-0}}$ represent the corresponding initial concentrations.

The DTG-6 yield and selectivity obtained by the two-step method were defined by

$$\text{DTG-6 yield in the two-step method: } Y_{4\text{-}6} = \frac{C_{\text{DTG-6}}}{C_{\text{DTG-4-0}}} \quad (7)$$

$$\text{DTG-6 selectivity in the two-step method: } S_{4\text{-}6} = \frac{Y_{4\text{-}6}}{X_{\text{DTG-4}}} \quad (8)$$

3. RESULTS AND DISCUSSION

3.1. Effect of the Solid Acid Type on the DTG-4 Deprotection in Microfluidized Bed. In our previous study, ACN was used as the solvent for the preparation of DTG-5 by the DTG-4 deprotection.[17] Hence, ACN was initially used as the solvent to study the effect of the solid acid catalyst on the

https://doi.org/10.1021/cbe.4c00139
Chem Bio Eng. 2025, 2, 182−191

reaction. First, the microfluidized bed with a length of 6 cm was loaded with 0.2 g of prepared solid acid catalyst, including Ti^{4+}-mont, SO_4^{2-}/TiO_2 solid acid, silica-supported methanesulfonic acid, and Na-mont, separately. The ACN solution containing 0.1 mol/L DTG-4 then was pumped into the microfluidized bed at a flow rate of 0.03 mL/min. After 50 min of continuous operation, samples were taken at the outlet end of the back pressure regulator for testing.

As shown in Table 1, Na-mont, SO_4^{2-}/TiO_2 solid acid, and the silica-supported methanesulfonic acid had no catalytic activity for the deprotection of DTG-4. The prepared catalysts were characterized with Brunauer–Emmett–Teller (BET) and pyridine adsorption Fourier transform infrared (Py-IR), respectively. Through the BET analysis, the pore diameters of the prepared catalysts were obtained (Figure S3). In addition, the catalyst acid type (i.e., Brønsted acid sites (BAS) and Lewis acid sites (LAS)) was assessed by Py-IR, and the ratio of BAS and LAS was determined by normalizing the peak area of the spectra (Figure S4). Bands at 1540 and 1450 cm^{-1} were observed in the spectra of all of the measured samples, indicating the coexistence of BAS and LAS in the catalysts. The absorption band near 1540 cm^{-1} was due to the formation of PyH^+ by protonation at BAS, whereas the absorption band near 1450 cm^{-1} was due to the ligand-bound pyridine with the LAS.[39] In addition, the absorption band at 1490 cm^{-1} was associated with the vibration of the pyridine ring on BAS and LAS. The peak near 1625 cm^{-1} is usually considered to be associated with physically absorbed pyridine due to the combination of hydrogen bonds and surface hydroxyl. Relevant data are provided in Table S1. Kim suggested that bulky compounds failed to pass through the small pores to combine with the acidic sites.[40] SO_4^{2-}/TiO_2 had a smaller pore size (Figure S3) and contained weaker acid sites than Ti^{4+}-mont (25.41 vs 60.46 μmol/g at 250 °C). These resulted in no catalytic activity of SO_4^{2-}/TiO_2 for DTG-4 deprotection. Although $MsOH/SiO_2$ exhibited a higher total concentration of BAS and LAS than Ti^{4+}-mont, its smaller pore size and higher B/L value (Table S1) hindered the catalysis of DTG-4 deprotection. Na-mont and Ti^{4+}-mont had a close pore size (4.1 nm). The parent Na-mont could not promote the DTG-4 deprotection, but Ti^{4+}-mont could smoothly transform acetal DTG-4 into aldehyde DTG-5. This indicated that the titanium introduction in the solid acid was an active acid component in this deprotection process,[33] which increased the total concentration of BAS and LAS. Although the interlayer space of Ti^{4+}-mont (2.7 Å) attested by its X-ray diffraction pattern was slightly smaller than that of the parent Na-mont (2.9 Å), it could be expanded when soaked in a solvent, such as DMSO (4.4 Å), propane-1,2-diol (8.4 Å), acetone/H_2O (17.5 Å), and ethylene glycol (7.2 Å).[36] The increased interlayer space facilitates the combination of bulky compounds with these acid sites.[41,42] Hence, from the experimental results, it was clear that Ti^{4+}-mont was the optimal heterogeneous catalyst for the following study.

Table 1. Effect of the Solid Acid Type in the Microfluidized Bed[a]

solid acid catalysts	conversion of DTG-4/%[b]	yield of DTG-5/%[b]
Ti^{4+}-mont	30.5	29.9
SO_4^{2-}/TiO_2	0	0
$MsOH/SiO_2$	0	0
Na-mont	0	0

[a]All reactions were carried out under the same conditions except for the solid acid: the temperature was 120 °C, and t_1 was 17 min. [b]DTG-4 conversion and DTG-5 yield were determined by HPLC using the external standard method.

3.2. Effect of the Solvent Type on the DTG-4 Deprotection in the Microfluidized Bed. During the deprotection of acetals, the cleavage of the carbonyl C–O bond is accompanied by the generation of the carbonium ion, which is recognized as the rate-determining step.[43] The carbonium ion generated in this step was much more stable in the polar solvents (i.e., proton solvents and dipole solvents) than in the nonpolar solvents. On the one hand, common proton solvents are water, ethanol, acetic acid, formic acid, and so on. Considering the solubility of the raw material DTG-4 (Table S2), water and ethanol were not considered as solvents. In addition, instead of choosing a strong organic acid (formic acid), we chose a weak organic acid (AcOH) as the solvent because of the need for a weak acidic solution in the next step (cyclization for the DTG-6 formation). On the other hand, common dipole solvents such as DMSO, DMF, ACN, acetone, etc., which have good solubility of DTG-4 (Table S2), were also considered. As shown in Table 2, studies of various solvents with the catalyst Ti^{4+}-mont revealed that the target product (DTG-5) could not be synthesized in DMSO, DMF, and acetone. Among these five solvents, the polarity of acetone is the minimum, leading to the failure of the DTG-4 deprotection. Although the polarities of DMSO and DMF are higher than those of AcOH and ACN, DMSO decomposes to methyl mercaptan and formaldehyde under acidic conditions,[44] and DMF correspondingly decomposes to dimethylamine and carbon monoxide.[45] Thus, DMF and DMSO also could not be applied as solvents for DTG-4 deprotection. Interestingly, the reaction rate of DTG-4 was faster when AcOH was used as the solvent compared to ACN, and both of them showed similar selectivity. Hence, AcOH as the solvent gave the best results for the formation of DTG-5.

Table 2. Effect of the Solvent[a]

solvent	conversion of DTG-4/%[b]	yield of DTG-5/%[b]
ACN	30.5	29.9
DMSO	17.8	0.7
acetone	0	0
DMF	0	0
AcOH	31.6	31.3

[a]All reactions were carried out under the same conditions except for the solvents: the mass of Ti^{4+}-mont was 0.2 g, and the temperature was 120 °C. [b]DTG-4 conversion and DTG-5 yield were determined by HPLC using the external standard method.

3.3. Effect of the Flow Rate in the Microfluidized Bed. Particle size distribution of Ti^{4+}-mont was analyzed by a Mastersizer 3000 laser particle size analyzer. The results are listed in Table 3. The D50 of the particle size was applied to represent the median diameter of the Ti^{4+}-mont catalyst particles.

When the particle Reynolds number (Re_p) is less than 20, the minimum fluidization velocity is determined using the following equation:[46]

$$u_{mf} = \frac{d_e^2(\rho_p - \rho)g}{1650\mu} \quad (9)$$

https://doi.org/10.1021/cbe.4c00139
Chem Bio Eng. 2025, 2, 182–191

Table 3. Particle Size Distribution of Ti^{4+}-mont[a]

sample number	D10	D50	D90
1	2.11	4.70	10.4
2	2.16	4.98	14.7
3	1.92	4.41	9.36
4	1.92	4.39	9.32
5	1.91	4.38	9.29
average	2.00	4.57	10.61
SD	0.12	0.26	2.33
RSD (%)	6.04	5.78	21.96

[a]D50 = 4.57 μm (D50 is the particle size for which the cumulative distribution percentage of the sample reaches 50% and is usually used to indicate the average particle size of the powder); SD, standard deviation; RSD, relative standard deviation.

where d_e is the average diameter of Ti^{4+}-mont particles (4.57×10^{-6} m), ρ_p is the density of Ti^{4+}-mont particles (2000 kg/m^3), ρ is the density of AcOH (941.71 kg/m^3 at 120 °C), g is the acceleration of gravity (9.81 m/s^2), and μ is the dynamic viscosity of AcOH (3.66×10^{-4} Pa s at 120 °C).

Here, the value of D50 was used to represent d_e. According to eq 9, the minimum fluidization velocity was calculated to be 3.59×10^{-7} m/s. With the steel column diameter of 4.6 mm, the minimum fluidization velocity was also expressed as 3.58×10^{-4} mL/min. According to eq 10, the particle Reynolds number regarding the minimum fluidization (Re_{pmf}) was determined to be 4.23×10^{-6}, which was much less than 20 meeting the assumptions of this calculation.

$$Re_{pmf} = \frac{d_e u_{mf} \rho}{\mu} \tag{10}$$

When the particle Reynolds number (Re_p) is less than 2, the settling velocity is determined using the following equation:[46]

$$u_t = \frac{d_e^2(\rho_p - \rho)g}{18\mu} \tag{11}$$

According to eq 11, the settling velocity was calculated to be 3.29×10^{-5} m/s. Accordingly, the settling velocity was also expressed as 0.033 mL/min with a steel column diameter of 4.6 mm. According to eq 12, the particle Reynolds number regarding the settling (Re_{pt}) was determined to be 3.9×10^{-4}, which was less than 2 meeting the assumptions of this calculation.

$$Re_{pt} = \frac{d_e u_t \rho}{\mu} \tag{12}$$

Once the apparent flow velocity reaches the settling velocity of particles, a large number of particles will be taken out of the reactor and cause blockage at the top of the microfluidized bed. Hence, the upper limit of the operating range in the microfluidized bed is the settling velocity of the particles. To further describe the motion of the particles inside the microfluidized bed, Ti^{4+}-mont stained with methylene blue was added into a quartz tube with 4.6 mm inner diameter, and two mesh screens were equipped at the ends of the quartz tube to fix the range of motion for the catalysts. When the flow rate was 0.03 mL/min, the catalyst particles were in a fluidized state (Figure S5b), indicating that the experimental results of the flow rate were consistent with the theoretical calculations. When the flow rate was 0.01 mL/min, bed expansion was observed (Figure S5a). When the flow rate was increased to 0.1 mL/min, most of the solid acid catalysts were hydraulically transported to the top of the microfluidized bed (see Figure S5c), and a small amount of the solid acid catalyst with large particle size (>4.57 μm, Table 3) deposited at the bottom of the microreactor required a higher fluidization velocity to fluidize.

When the flow rate was 0.03 mL/min, the pressure drop over the microreactor system was 0.9 MPa, while for 0.06 mL/min, the pressure drop over the microreactor was 2 MPa. In this case, the catalyst particles accumulated at the top of the steel column, causing clogging, and thus did not maintain stable fluidization, which was not conducive to the full contact between the catalysts and the solution. Therefore, the flow rate was selected as 0.03 mL/min.

3.4. Effect of the Temperature in the Microfluidized Bed. Since the DTG-5 selectivity was maintained at about 99% in the experiments, the influence of temperature on the DTG-4 conversion during the DTG-4 deprotection was independently investigated. Figure 3 demonstrates the increase of DTG-4 conversion with increasing reaction temperature until 120 °C. After removing Ti^{4+}-mont from the reaction system, it was found that the color of Ti^{4+}-mont changed from off-white to pale yellow due to the adsorption of the compounds during the DTG-4 deprotection. However, a further increase of the temperature resulted in the slight decrease of the DTG-4 conversion. At a reaction temperature of 125 °C for 5 h running, the catalyst Ti^{4+}-mont turned brown after being removed from the reaction system. The deactivated and fresh Ti^{4+}-mont were tested separately by inductively coupled plasma-mass spectrometry (ICP-MS), which revealed a negligible change (1.1%) in the Ti content of the catalysts. Subsequently, the catalysts were analyzed by transmission electron microscopy (TEM), as shown in Figure S6. It was found that the deactivated Ti^{4+}-mont showed sintered crystallites with larger particle sizes in addition to smaller isolated particles, suggesting that the catalyst was deactivated due to sintering. Therefore, the optimal reaction temperature was 120 °C under the experimental conditions.

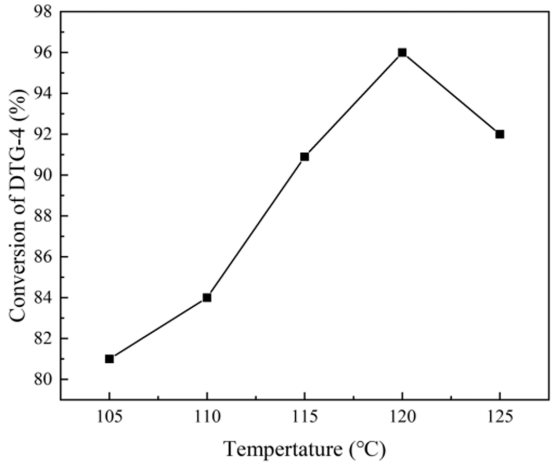

Figure 3. Effect of the temperature in the microfluidized bed: 0.4 g of Ti^{4+}-mont.

Nqeketo et al.[16] obtained 100% DTG-4 conversion and 48% DTG-5 selectivity using 0.01 mol/L DTG-4 solution in a packed-bed reactor filled with 2.6 g of acid resin catalyst. Interestingly, when the residence time of DTG-4 deprotection

https://doi.org/10.1021/cbe.4c00139
Chem Bio Eng. 2025, 2, 182−191

(t_1) was 50 min, 97% DTG-4 conversion and 99% DTG-5 selectivity were obtained using 0.1 mol/L DTG-4 reaction solution in a microfluidized bed containing 0.4 g of solid acid catalyst at 120 °C in our work. Therefore, compared with the acidic resin catalysts, Ti^{4+}-mont was selected as the catalyst to reduce the consumption of solvent and catalyst, which is beneficial for the efficient synthesis of DTG-5.

3.5. Effect of the Solvent on the DTG-5 Cyclization. In order to simplify the optimization of the conditions for the DTG-5 cyclization, purified DTG-5 was dissolved in the solvent and reacted with the RABO solution at 135 °C to prepare DTG-6 in this section. In the above study, it was determined that the flow rate of the solution containing DTG-5 was 0.03 mL/min. Therefore, in the separate DTG-5 cyclization process, the flow rates of both streams containing DTG-5 and RABO were set to 0.03 mL/min to ensure adequate mixing. The solvent of DTG-4 deprotection was AcOH, which might react with RABO to generate a byproduct. The byproduct (named AR) formation was confirmed in subsequent work. Hence, we need to further optimize the solvent for DTG-5 cyclization.

ACN was generally used as the solvent for the DTG-5 cyclization.[17] Thus, a mixture of ACN and AcOH was employed as the solvent to minimize AR in this work. The influence of the volume ratio of AcOH in the mixed solvent on the DTG-5 cyclization was studied and displayed in Figure 4.

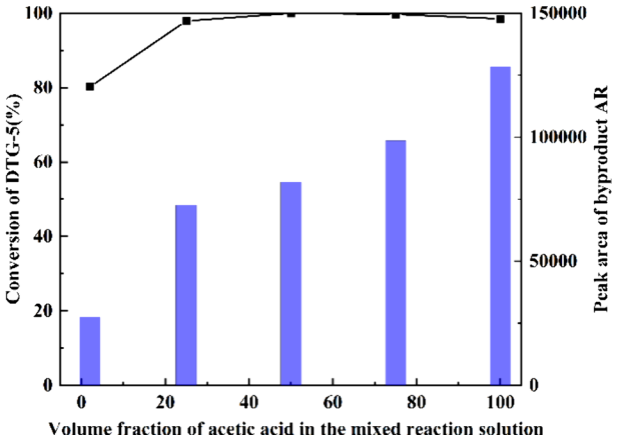

Figure 4. Effect of the volume fraction of acetic acid/mixed solution on DTG-5 cyclization: C_{DTG-5} was 0.2 mol/L, the molar ratio of RABO/DTG-5 was 1.1, and t_2 was 20 min.

When the volumetric fraction of AcOH increased from 2% to 50%, it was clearly observed that the DTG-5 conversion increased from 80.2% to 99.9%, indicating that AcOH could improve the reaction rate of DTG-5 cyclization and shorten the reaction time. However, the DTG-5 conversion showed a gradual decrease with a further increasing AcOH volumetric fraction. Meanwhile, the peak area of AR, which is proportional to the concentration of AR, showed an increasing trend with the increase in the AcOH volumetric fraction. This suggested that a portion of RABO was consumed by AcOH to generate the byproduct AR, which explained the reduction of DTG-5 conversion at a high concentration of AcOH as a solvent. Considering the reaction time and the selectivity, the optimum volume fraction of the AcOH/mixed solution was 50%. This means that AcOH solution (solution A) containing DTG-5 and ACN solution (solution B) containing RABO are mixed in a 1:1 volume ratio in a subsequent operation to undergo DTG-5 cyclization.

3.6. Effect of the RABO/DTG-5 Molar Ratio on the DTG-5 Cyclization. To balance the reaction time and consumption of RABO in the DTG-5 cyclization, the influence of the molar ratio of RABO to DTG-5 on the yield and selectivity of DTG-6 was investigated. As shown in Figure 5,

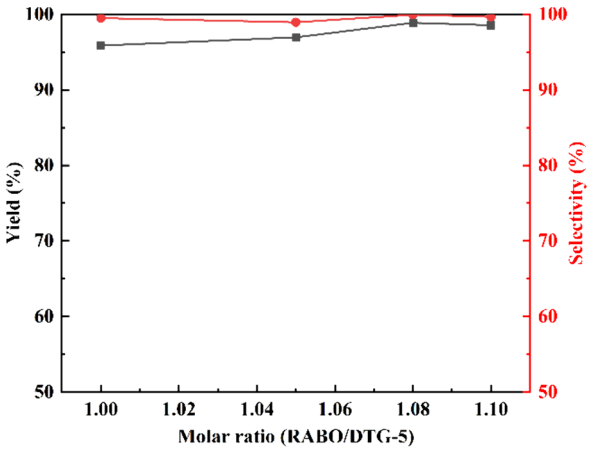

Figure 5. Effect of the molar ratio of RABO/DTG-5: t_2 was 20 min.

the DTG-6 selectivity remained above 99%, indicating that there was no side reaction occurring during the DTG-5 cyclization. Meanwhile, as the molar ratio of RABO to DTG-5 increased from 1 to 1.08, the corresponding DTG-6 yield increased from 95.86% to 98.87%. The DTG-6 yield then remained essentially constant, as the molar ratio of RABO to DTG-5 continued to increase. Therefore, the optimal molar ratio of RABO to DTG-5 was 1.08 to promote the reaction and reduce the consumption of RABO.

3.7. Kinetic Calculation in the DTG-5 Cyclization. To gain a profound understanding and optimize the process, a kinetic study of the DTG-5 cyclization is presented for the first time. The effects of the residence time and reaction temperature on DTG-5 conversion and DTG-6 yield were investigated in the microreactor. According to Figure 6, DTG-6 selectivity was above 99% at various experimental conditions, proving that the reaction of AcOH with RABO could be neglected after screening the reaction conditions. When the temperature increased from 95 to 135 °C at the same residence time of 10 min, the DTG-5 conversion was notably raised from 54.9% to 99.0%, and the corresponding DTG-6 yield was improved from 54.8% to 98.7%. Overall, increasing the reaction temperature significantly reduced the reaction time without side reactions. When the reaction temperature was 135 °C, the reaction time was shortened to 10 min, which is much less than the existing batch time (18.5 h) and reported reaction time of the continuous-flow process (25 min).[17,47] When the reaction temperature was further increased, gases were produced by evaporation of the solvent in the microchannel at a pressure of 2.76 bar. Therefore, the optimal value of the reaction temperature was 135 °C, taking into account the minimum reaction time.

The reaction rate of DTG-5 cyclization was described as

$$r_{DTG-6} = \frac{dC_{DTG-6}}{dt} = kC_{DTG-5}^{\alpha}C_{RABO}^{\beta} \quad (13)$$

https://doi.org/10.1021/cbe.4c00139
Chem Bio Eng. 2025, 2, 182−191

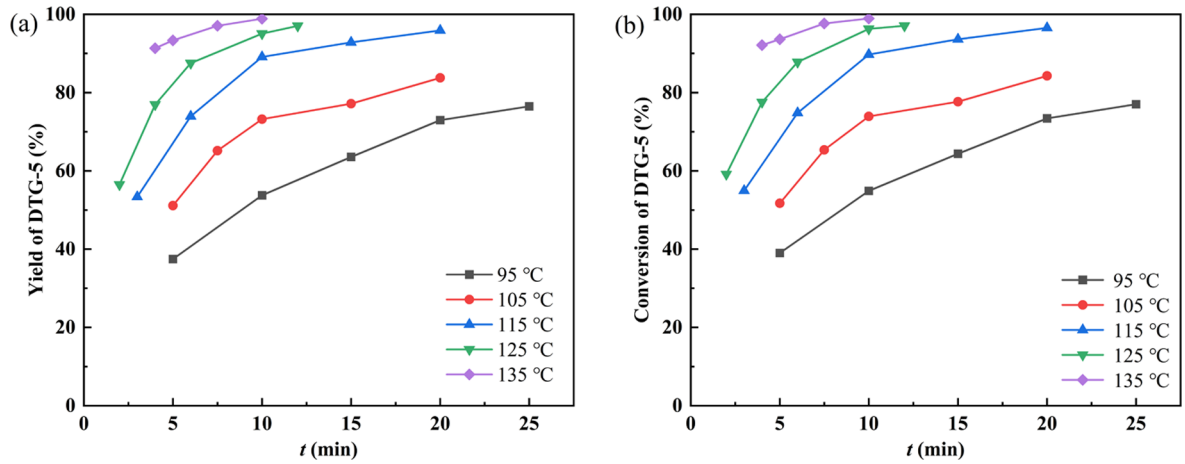

Figure 6. Effects of the residence time and temperature on (a) the conversion of DTG-5 and (b) the yield of DTG-6. The molar ratio of RABO/DTG-5 was 1.08, and $C_{DTG\text{-}5}$ was 0.2 mol/L.

where k is the reaction rate constant for the DTG-5 cyclization, C_{RABO} is the concentration of RABO (mol/L), and α and β are the reaction orders corresponding to DTG-5 and RABO, respectively.

Experimental data obtained above were processed by MATLAB R2019b software to obtain the kinetic parameters (k, α, and β) at various reaction temperatures. The calculated reaction orders of DTG-5 and RABO were both 1, indicating that the DTG-5 cyclization is a second-order reaction. Table 4 shows the calculated k values at various temperatures.

Table 4. Values of k at Different Temperatures

temp (°C)	95	105	115	125
k (L/(mol^{-1} min^{-1}))	0.017	0.033	0.071	0.135

According to the Arrhenius equation, the rate constant is expressed as a function of temperature by eq 14:

$$\ln k = \ln A - \frac{E_a}{R} \times \frac{1}{T} \tag{14}$$

where A is the pre-exponential factor of DTG-5 cyclization, R is the gas constant (8.314 J K^{-1} mol^{-1}), and E_a is the activation energy (kJ mol^{-1}) of DTG-5 cyclization. From the data in Table 4, the correlation coefficient (R^2) of fitting ln k to $1/T$ was calculated to be greater than 0.99 (Figure S7), and the pre-exponential factor A and the activation energy E_a were 1.95 × 10^{10} L/(mol^{-1} min^{-1}) and 84.0 kJ mol^{-1}, respectively.

The developed kinetic model was used to predict the behavior of DTG-5 cyclization at a reaction temperature of 135 °C. Figure 7 indicated that the kinetic model was reliable, as the error between the experimental data and the predicted data was within 10%. This also suggested that if the reaction conditions are further optimized to increase the DTG-5 concentration during subsequent studies, the reaction time can be predicted based on the initial DTG-5 concentration and the reaction temperature to improve the operational efficiency.

3.8. Assessment of Two-Step Synthesis of DTG-6 from DTG-4 in the Microfluidized Bed Cascade System. Both the DTG-4 deprotection and the DTG-5 cyclization obtained satisfactory yields and selectivities when studied independently. Next, the DTG-4 deprotection and the DTG-5 cyclization were operated in tandem in the microreactor system, in which a microfluidized bed was constructed for the

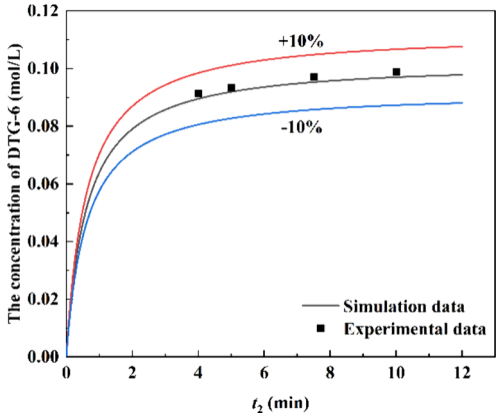

Figure 7. Kinetic model validation at a temperature of 135 °C.

first time with the heterogeneous catalyst. After the DTG-4 deprotection, DTG-5 was produced at a concentration of 0.096 mol/L, and the corresponding RABO concentration was calculated to be 0.104 mol/L based on the optimal molar ratio of RABO/DTG-5. After mixing the two aforementioned reaction streams, the concentrations of DTG-5 and RABO were 0.048 and 0.052 mol/L, respectively. According to the established kinetic model, after determination of the initial concentration of the reactants and the reaction temperature, the residence time of DTG-5 cyclization can be calculated to be 26 min when the DTG-5 conversion is 99%. When the residence time of DTG-4 deprotection in the microfluidized bed was 50 min (t_1) and the residence time of DTG-5 cyclization was 26 min (t_2), it was experimentally verified that the yield of DTG-6 was 95% and the selectivity of the total reaction (from DTG-4 to DTG-6) was 98%. Herein, the total residence time t_3 for the two-step synthesis of DTG-6 was 80 min.

The stability of the microfluidized bed is of importance when considering its long running. The effect of the operational time on the synthesis of DTG-5 was studied in the microfluidized bed. The DTG-5 yield first was improved from 82% to 96% by increasing the operational time from 1 to 3 h and then was almost maintained stable from 3 to 18 h, as shown in Figure S8. These results implied that the catalyst Ti^{4+}-mont could adsorb a part of the product DTG-5 during the catalytic process. Such absorbance was also demonstrated

https://doi.org/10.1021/cbe.4c00139
Chem Bio Eng. 2025, 2, 182−191

by the change in the color of Ti^{4+}-mont from off-white to pale yellow. However, the DTG-5 yield decreased with further extension of the operation time. After the operational time of 18 h, the catalyst Ti^{4+}-mont gradually lost activity. The Ti^{4+}-mont was then washed with ACN and immersed in deionized water for 5 h. It was dried at 110 °C for 10 h and then could be reused for 6 h.

Environmental factors (E factor) and atom economy (AE) are the two most popular green metrics used to judge the greenness in a chemical process. To emphasize the importance of reducing the amount of waste generated during the process,[48] Trost introduced the concept of AE,[49] defined as the percentage of the molecular weight of the product versus the total molecular weight of reactants involved in the reaction. AE is a theoretical value without considering the yield and solvent consumption.[50] In contrast, E factor, which was defined as the following, is the more accurate assessment of the whole chemical process than AE by taking into account the yield of the target product as well as the waste from other auxiliary parts:[51]

$$\text{E factor} = \frac{\text{mass of total waste}}{\text{mass of product}} \quad (15)$$

where the mass of the product means the mass of DTG-6, and the mass of total waste includes the mass of the corresponding consumed solvent, reactants, catalyst, the reagents for product purification, and so on.

According to the definition of E factor, E factor for the new two-step method synthesizing DTG-6 in microfluidized bed cascade system was 59.6, which was within the normal range of the pharmaceuticals (25 to >100).[50] When the concentration of DTG-4 was equal to that of the present work, the E factor of the two-step method utilizing homogeneous catalyst in the cascade microreactor was 113.1. It is evident that the use of heterogeneous solid acid catalysts and the microfluidized bed cascade system achieves higher DTG-6 yield and is more compatible with green production than homogeneous catalysts.

4. CONCLUSIONS

This study was the first to use heterogeneous catalyst, that is, solid acid, in the microfluidized bed reactor to catalyze acetal deprotection. The reaction solution was directly reacted with RABO, avoiding the addition of base, to obtain a high DTG-6 yield (95%) in the cascade microreactor system. The effects of solid acid, solvent, temperature, and flow rate on DTG-4 deprotection were discussed carefully. Under the optimal experimental conditions, the independent yield and selectivity of DTG-5 were 96% and 99%, respectively. Subsequently, DTG-5 cyclization experiments were performed to discuss the DTG-5 conversion and the DTG-6 yield under various conditions, including the solvent, temperature, residence time, and molar ratio of RABO/DTG-5. Based on the experimental data, the kinetic model of DTG-5 cyclization was established and verified. The new two-step synthesis rapidly increased the total DTG-6 yield from 90% to 95%. In contrast, the corresponding E factor was rapidly reduced from 113.1 to 59.6, which means less waste. The microfluidized bed cascade system in this Article had a throughput of 26.3 mg/h for the DTG-6 synthesis, while on a production scale a throughput of g/h or more is required. Although our work had a higher yield of DTG-6 than that in the literature, the productivity for the microfluidized bed cascade system in this work needs to be enhanced by scale-up methods (e.g., sizing-up and numbering-up) to achieve industrial requirement.

■ ASSOCIATED CONTENT

Supporting Information

The Supporting Information is available free of charge at https://pubs.acs.org/doi/10.1021/cbe.4c00139.

Additional experimental details, and methods, including characterization data and performance details (PDF)

■ AUTHOR INFORMATION

Corresponding Authors

Minjing Shang − *School of Chemistry and Chemical Engineering, Key Laboratory of Thin Film and Microfabrication (Ministry of Education), Shanghai Jiao Tong University, Shanghai 200240, People's Republic of China*; Email: mshang@sjtu.edu.cn

Yuanhai Su − *School of Chemistry and Chemical Engineering, Key Laboratory of Thin Film and Microfabrication (Ministry of Education), Shanghai Jiao Tong University, Shanghai 200240, People's Republic of China*; orcid.org/0000-0002-0718-301X; Email: y.su@sjtu.edu.cn

Authors

Xiao Xue − *School of Chemistry and Chemical Engineering, Key Laboratory of Thin Film and Microfabrication (Ministry of Education), Shanghai Jiao Tong University, Shanghai 200240, People's Republic of China*; orcid.org/0000-0001-5788-2460

Chengmin Xie − *School of Chemistry and Chemical Engineering, Key Laboratory of Thin Film and Microfabrication (Ministry of Education), Shanghai Jiao Tong University, Shanghai 200240, People's Republic of China*

Guozhi Qian − *School of Chemistry and Chemical Engineering, Key Laboratory of Thin Film and Microfabrication (Ministry of Education), Shanghai Jiao Tong University, Shanghai 200240, People's Republic of China*

Min Qiu − *School of Chemistry and Chemical Engineering, Key Laboratory of Thin Film and Microfabrication (Ministry of Education), Shanghai Jiao Tong University, Shanghai 200240, People's Republic of China*

Rongkun Jiang − *State Key Laboratory of Bioreactor Engineering, Shanghai Key Laboratory of Chemical Biology, School of Pharmacy, East China University of Science and Technology, Shanghai 200237, People's Republic of China*

Mohsin Pasha − *School of Chemistry and Chemical Engineering, Key Laboratory of Thin Film and Microfabrication (Ministry of Education), Shanghai Jiao Tong University, Shanghai 200240, People's Republic of China*

Zihao Zhong − *School of Chemistry and Chemical Engineering, Key Laboratory of Thin Film and Microfabrication (Ministry of Education), Shanghai Jiao Tong University, Shanghai 200240, People's Republic of China*

Zhijun Wang − *Shanghai Desano Pharmaceuticals Co., Ltd., Shanghai 201203, People's Republic of China*

Shu Liu − *Shanghai Desano Pharmaceuticals Co., Ltd., Shanghai 201203, People's Republic of China*

Hua Zhang − *Shanghai Desano Pharmaceuticals Co., Ltd., Shanghai 201203, People's Republic of China*

Complete contact information is available at: https://pubs.acs.org/10.1021/cbe.4c00139

Notes

The authors declare no competing financial interest.

■ ACKNOWLEDGMENTS

We would like to acknowledge financial support from the National Natural Science Foundation of China (no. 22178215) and the Shanghai Commission of Science and Technology.

■ REFERENCES

(1) UNAIDS. *The Path That Ends AIDS: UNAIDS Global AIDS Update 2023*; Joint United Nations Programme on HIV/AIDS, 2023.
(2) Craigie, R. The molecular biology of HIV integrase. *Future Virol* **2012**, *7* (7), 679−686.
(3) Ballantyne, A. D.; Perry, C. M. Dolutegravir: first global approval. *Drugs* **2013**, *73* (14), 1627−1637.
(4) Deeks, S. G.; Kar, S.; Gubernick, S. I.; Kirkpatrick, P. Raltegravir. *Nat. Rev. Drug Discovery* **2008**, *7* (2), 117−118.
(5) Cihlar, T.; Fordyce, M. Current status and prospects of HIV treatment. *Curr. Opin Virol* **2016**, *18*, 50−56.
(6) Scarsi, K. K.; Havens, J. P.; Podany, A. T.; Avedissian, S. N.; Fletcher, C. V. HIV-1 integrase inhibitors: a comparative review of efficacy and safety. *Drugs* **2020**, *80* (16), 1649−1676.
(7) Lepik, K. J.; Yip, B.; Ulloa, A. C.; Wang, L.; Toy, J.; Akagi, L.; Lima, V. D.; Guillemi, S.; Montaner, J. S. G.; Barrios, R. Adverse drug reactions to integrase strand transfer inhibitors. *AIDS* **2018**, *32* (7), 903−912.
(8) Anstett, K.; Brenner, B.; Mesplede, T.; Wainberg, M. A. HIV drug resistance against strand transfer integrase inhibitors. *Retrovirology* **2017**, *14* (1), 36.
(9) Wang, H.; Kowalski, M. D.; Lakdawala, A. S.; Vogt, F. G.; Wu, L. An efficient and highly diastereoselective synthesis of GSK1265744, a potent HIV integrase inhibitor. *Org. Lett.* **2015**, *17* (3), 564−567.
(10) Ohta, R.; Matsumoto, N.; Ueyama, Y.; Kuboki, Y.; Aoyama, H.; Murai, K.; Arisawa, M.; Maegawa, T.; Fujioka, H. Highly discriminative and chemoselective deprotection/transformations of acetals with the combination of trialkylsilyl triflate/2,4,6-collidine. *J. Org. Chem.* **2018**, *83* (12), 6432−6443.
(11) Saravanan, P.; Chandrasekhar, M.; Vijaya Anand, R.; Singh, V. K. An efficient method for deprotection of acetals. *Tetrahedron Lett.* **1998**, *39* (19), 3091−3092.
(12) Sun, J.; Dong, Y.; Cao, L.; Wang, X.; Wang, S.; Hu, Y. Highly efficient chemoselective deprotection of O,O-acetals and O,O-ketals catalyzed by molecular iodine in acetone. *J. Org. Chem.* **2004**, *69* (25), 8932−8934.
(13) Eash, K. J.; Pulia, M. S.; Wieland, L. C.; Mohan, R. S. A simple chemoselective method for the deprotection of acetals and ketals using bismuth nitrate pentahydrate. *J. Org. Chem.* **2000**, *65* (24), 8399−8401.
(14) Ziegler, R. E.; Desai, B. K.; Jee, J. A.; Gupton, B. F.; Roper, T. D.; Jamison, T. F. 7-step flow synthesis of the HIV integrase inhibitor dolutegravir. *Angew. Chem., Int. Ed.* **2018**, *57* (24), 7181−7185.
(15) Wang, X.; Chen, S.; Cui, H.; He, Y.; Zhao, C. Three-step synthetic procedure to prepare dolutegravir, cabotegravir, and bictegravir. *Green Chem. Lett. Rev.* **2022**, *15* (2), 312−319.
(16) Nqeketo, S.; Watts, P. Synthesis of dolutegravir exploiting continuous flow chemistry. *J. Org. Chem.* **2023**, *88* (16), 12024−12040.
(17) Xue, X.; Jiang, R.; Xie, C.; Qian, G.; Shang, M.; Zhu, W.; Su, Y. Mechanism and kinetic study for the intensification of two-step synthesis of a dolutegravir intermediate in microreactor. *AIChE J.* **2022**, *68* (11), No. e17820.
(18) Dawes, G. J. S.; Scott, E. L.; Le Nôtre, J.; Sanders, J. P. M.; Bitter, J. H. Deoxygenation of biobased molecules by decarboxylation and decarbonylation − a review on the role of heterogeneous, homogeneous and bio-catalysis. *Green Chem.* **2015**, *17* (6), 3231−3250.
(19) Jayakumar, M.; Karmegam, N.; Gundupalli, M. P.; Bizuneh Gebeyehu, K.; Tessema Asfaw, B.; Chang, S. W.; Ravindran, B.; Kumar Awasthi, M. Heterogeneous base catalysts: Synthesis and application for biodiesel production - A review. *Bioresour. Technol.* **2021**, *331*, No. 125054.
(20) Mansir, N.; Teo, S. H.; Rabiu, I.; Taufiq-Yap, Y. H. Effective biodiesel synthesis from waste cooking oil and biomass residue solid green catalyst. *Chem. Eng. J.* **2018**, *347*, 137−144.
(21) Ma, D.; Zhu, C.; Fu, T.; Ma, Y.; Yuan, X. Performance and pressure drop of CO_2 absorption into task-specific and halide-free ionic liquids in a microchannel. *AIChE J.* **2022**, *68* (6), 1 DOI: 10.1002/aic.17613.
(22) Chen, Q.; An, Y.; Feng, M.; Li, J.; Li, Y.; Tong, F.; Qu, G.; Sun, Z.; Wang, Y.; Luo, G. An enzyme-assembled gel monolithic microreactor for continuous flow asymmetric synthesis of aryl alcohols. *Green Chem.* **2022**, *24* (24), 9508−9518.
(23) Chen, Y.; Zhao, Y.; Han, M.; Ye, C.; Dang, M.; Chen, G. Safe, efficient and selective synthesis of dinitro herbicidesvia a multifunctional continuous-flow microreactor: one-step dinitration with nitric acid as agent. *Green Chem.* **2013**, *15* (1), 91−94.
(24) Scott, D. S.; Piskorz, J. Low rate entrainment feeder for fine solids. *Industrial & Engineering Chemistry Fundamentals* **1982**, *21* (3), 319−322.
(25) Potic, B.; Kersten, S. R. A.; Ye, M.; Van Der Hoef, M. A.; Kuipers, J. A. M.; Van Swaaij, W. P. M. Fluidization with hot compressed water in micro-reactors. *Chem. Eng. Sci.* **2005**, *60* (22), 5982−5990.
(26) Liu, X.; Xu, G.; Gao, S. Micro fluidized beds: Wall effect and operability. *Chem. Eng. J.* **2008**, *137* (2), 302−307.
(27) Yu, J.; Yao, C.; Zeng, X.; Geng, S.; Dong, L.; Wang, Y.; Gao, S.; Xu, G. Biomass pyrolysis in a micro-fluidized bed reactor: Characterization and kinetics. *Chem. Eng. J.* **2011**, *168* (2), 839−847.
(28) Fang, Y.; Zou, R.; Luo, G.; Chen, J.; Li, Z.; Mao, Z.; Zhu, X.; Peng, F.; Guo, S.; Li, X.; et al. Kinetic study on coal char combustion in a microfluidized bed. *Energy Fuels* **2017**, *31* (3), 3243−3252.
(29) Li, C.; Ma, Y.; Liu, M. Comprehensive investigations on flow field in liquid-solid mini-fluidized beds. *Powder Technol.* **2023**, *429*, 118898.
(30) Sagmeister, P.; Lebl, R.; Castillo, I.; Rehrl, J.; Kruisz, J.; Sipek, M.; Horn, M.; Sacher, S.; Cantillo, D.; Williams, J. D.; et al. Advanced Real-Time Process Analytics for Multistep Synthesis in Continuous Flow*. *Angew. Chem., Int. Ed.* **2021**, *60* (15), 8139−8148.
(31) Sacher, S.; Castillo, I.; Rehrl, J.; Sagmeister, P.; Lebl, R.; Kruisz, J.; Celikovic, S.; Sipek, M.; Williams, J. D.; Kirschneck, D.; et al. Automated and continuous synthesis of drug substances. *Chem. Eng. Res. Des.* **2022**, *177*, 493−501.
(32) Sagandira, M. B.; Sagandira, C. R.; Watts, P. Continuous flow synthesis of xylidines via biphasic nitration of xylenes and nitro-reduction. *J. Flow Chem.* **2021**, *11* (2), 193−208.
(33) Mitsudome, T.; Matsuno, T.; Sueoka, S.; Mizugaki, T.; Jitsukawa, K.; Kaneda, K. Direct synthesis of unsymmetrical ethers from alcohols catalyzed by titanium cation-exchanged montmorillonite. *Green Chem.* **2012**, *14* (3), 610−613.
(34) Kawabata, T.; Kato, M.; Mizugaki, T.; Ebitani, K.; Kaneda, K. Highly efficient deprotection of acetals by titanium cation-exchanged montmorillonite as a strong solid acid catalyst. *Chem. Lett.* **2003**, *32* (7), 648−649.
(35) Kawabata, T.; Mizugaki, T.; Ebitani, K.; Kaneda, K. Highly efficient heterogeneous acetalization of carbonyl compounds catalyzed by a titanium cation-exchanged montmorillonite. *Tetrahedron Lett.* **2001**, *42*, 8329−8332.
(36) Ebitani, K.; Kawabata, T.; Nagashima, K.; Mizugaki, T.; Kaneda, K. Simple and clean synthesis of 9,9-bis[4-(2-hydroxyethoxy)phenyl] fluorene from the aromatic alkylation of

phenoxyethanol with fluoren-9-one catalysed by titanium cation-exchanged montmorillonite. *Green Chem.* **2000**, *2* (4), 157−160.
(37) Song, X.; Wang, Y.; Song, D.; An, C.; Wang, J. Catalysis of a nanometre solid super acid of SO_4^{2-}/TiO2 on the thermal decomposition of ammonium nitrate. *Nanomater. Nanotechnol.* **2016**, *6*, 23.
(38) Ren, L.; Zhang, X.; Gao, W. Synthesis of biodiesel via transesterification over silica-supported methanesulfonic acid. *Ind. Catal.* **2009**, *17*, 40−44.
(39) Jin, F.; Li, Y. A FTIR and TPD examination of the distributive properties of acid sites on ZSM-5 zeolite with pyridine as a probe molecule. *Catal. Today* **2009**, *145* (1), 101−107.
(40) Kim, K.; Lee, T.; Kwon, Y.; Seo, Y.; Song, J.; Park, J. K.; Lee, H.; Park, J. Y.; Ihee, H.; Cho, S. J.; et al. Lanthanum-catalysed synthesis of microporous 3D graphene-like carbons in a zeolite template. *Nature* **2016**, *535* (7610), 131−135.
(41) Ballini, R.; Bosica, G.; Frullanti, B.; Maggi, R.; Sartori, G.; Schroer, F. 1,3-Dioxolanes from carbonyl compounds over zeolite HSZ-360 as a reusable, heterogeneous catalyst. *Tetrahedron Lett.* **1998**, *39* (12), 1615−1618.
(42) Corma, A.; Climent, M. J.; Carcía, H.; Primo, J. Formation and hydrolysis of acetals catalysed by acid Faujasites. *Appl. Catal.* **1990**, *59* (1), 333−340.
(43) Stasiuk, F.; Sheppard, W. A.; Bourns, A. N. An oxygen-18 study of acetal formation and hydrolysis. *Can. J. Chem.* **1956**, *34* (2), 123−127.
(44) Santosusso, T. M.; Swern, D. Acid catalysis as a basis for a mechanistic rationale of some dimethyl sulfoxide reactions. *Tetrahedron Lett.* **1974**, *15* (48), 4255−4258.
(45) Muzart, J. N,N-Dimethylformamide: much more than a solvent. *Tetrahedron* **2009**, *65* (40), 8313−8323.
(46) Davidson, J. F.; Clift, R.; Harrison, D. *Fluidization*; Academic Press: New York, 1985.
(47) Hughes, D. L. Review of synthetic routes and final forms of integrase inhibitors dolutegravir, cabotegravir, and bictegravir. *Org. Process Res. Dev.* **2019**, *23* (5), 716−729.
(48) Pitzer, J.; Steiner, K.; Schmid, C.; Schein, V. K.; Prause, C.; Kniely, C.; Reif, M.; Geier, M.; Pietrich, E.; Reiter, T.; et al. Racemization-free and scalable amidation of L-proline in organic media using ammonia and a biocatalyst only. *Green Chem.* **2022**, *24* (13), 5171−5180.
(49) Trost, B. M. Atom economy—a challenge for organic synthesis: homogeneous catalysis leads the way. *Angew. Chem., Int. Ed.* **1995**, *34* (3), 259−281.
(50) Sheldon, R. A. The E factor 25 years on: the rise of green chemistry and sustainability. *Green Chem.* **2017**, *19* (1), 18−43.
(51) Centi, G.; Perathoner, S. Catalysis and sustainable (green) chemistry. *Catal. Today* **2003**, *77* (4), 287−297.

https://doi.org/10.1021/cbe.4c00139
Chem Bio Eng. 2025, 2, 182−191